Revision 1

Fe-Mg interdiffusion in orthopyroxene

Ralf Dohmen[#,*], Jan H. Ter Heege[$], Hans-Werner Becker[†] and Sumit Chakraborty[#,†]

[#]Institute for Geology, Mineralogy and Geophysics,
Ruhr-University Bochum, 44801 Bochum, Germany
email: ralf.dohmen@ruhr-uni-bochum.de
phone: ++49-234 3224394
fax: ++49-234 3214433

[$] present address: TNO,
Utrecht, Netherlands

[†]RUBION,
Ruhr-University Bochum, 44801 Bochum,
[*]Corresponding author

keywords: orthopyroxene, Fe-Mg diffusion, diffusion chronometry, geothermometry, cooling rates

Abstract

We have measured Fe-Mg interdiffusion coefficients, $D_{Fe\text{-}Mg}$, parallel to the three main crystallographic axes in two natural orthopyroxene single crystals [approximately $En_{98}Fs_1$ (X_{Fs} = X_{Fe} = 0.01) and $En_{91}Fs_9$] using diffusion couples consisting of a 20 - 90 nm thick silicate thin film deposited under vacuum on polished and oriented pyroxene single crystals. The thin films were prepared using pulsed laser ablation of polycrystalline olivine pellets (composition: $Fo_{30}Fa_{70}$). Samples were annealed for 4 - 337 hours at 870 - 1100 °C under atmospheric pressure in a continuous flow of CO + CO_2 to control the oxygen fugacity, fO_2, between 10^{-11} and 10^{-7} Pa within the stability field of pyroxene. Film thickness and compositional profiles were measured using Rutherford Backscattering Spectroscopy (RBS) on reference and annealed samples, and Fe concentration depth profiles were extracted from the RBS spectra and fitted numerically considering a compositional dependence of $D_{Fe\text{-}Mg}$ in orthopyroxene. We obtain an Arrhenius relationship for both types of crystals, but only for the more Fe-rich composition a dependence on fO_2 could be clearly identified. For diffusion along [001] in the composition Fs_9, least squares regression of the log $D_{Fe\text{-}Mg}$ vs. reciprocal temperature yields the following Arrhenius equation:

$$D_{Fe\text{-}Mg}\ [m^2/s] = 1.12\ 10^{-6}\ (fO_2\ [Pa])^{0.053 \pm 0.027}\ \exp(-308 \pm 23\ [kJ/mol]/(RT)).$$

$D_{Fe\text{-}Mg}$ in opx with X_{Fe} = 0.01 obeys a relationship that does not depend on fO_2:

$$D_{Fe\text{-}Mg}\ [m^2/s] = 1.66\ 10^{-4}\ \exp(-377 \pm 30\ [kJ/mol]/(RT)).$$

Diffusion along [001] is faster than diffusion along [100] by a factor of 3.5, while diffusion along [010] is similar to that along [001]. Comparison of $D_{Fe\text{-}Mg}$ and rates of order-disorder kinetics indicates that for fO_2 around the IW buffer and lower, diffusion in natural orthopyroxene becomes insensitive to fO_2, which could be related to a transition in the diffusion mechanism from a transition metal extrinsic (TaMED) domain to a pure extrinsic (PED) domain. This behavior is analogous to that observed for Fe-Mg diffusion in olivine and this complexity

precludes the formulation of a closed form expression for the composition and fO_2 dependence of $D_{Fe\text{-}Mg}$ in orthopyroxene at present. We were not able to quantitatively constrain the dependence of $D_{\mathrm{Fe\text{-}Mg}}$ on the X_{Fs} content from the profile shapes, but consideration of the experimentally measured diffusion coefficients along with the data for order-disorder kinetics suggests that the compositional dependence is weaker than previously estimated, at least for orthopyroxenes with $X_{\mathrm{Fe}} < 0.5$. For the major element compositional, T and fO_2 range of available experimental data, Fe-Mg interdiffusion in orthopyroxene is slower than in olivines and spinels, comparable to garnet, and faster than in clinopyroxenes.

Introduction

Fe-Mg interdiffusion in silicate minerals is of interest in petrological studies for determining the closure temperature of geothermometers and for determining cooling rates or durations of processes such as residence times at peak metamorphic conditions or in magma chambers (e.g., Dodson, 1973; Lasaga, 1983; Dodson 1986; Ganguly and Tirone, 1999). Fe-Mg diffusion in orthopyroxene has been used to infer these parameters (e.g., Smith and Barron, 1991; Pattison and Begin, 1994; Rietmeijer and Champness 1982) as well as to determine crystal residence times in magmas from compositional profiles (e.g., Saunders et al. 2012, Allan et al. 2013, Chamberlain et al. 2014), and thermal histories of meteorites (e.g., Ganguly et al. 2013). It is also relevant for studies of the physical properties of silicates, such as rheology or electrical conductivity (Mackwell 1991; Skemer and Karato, 2007; Dai and Karato, 2009; Farla et al. 2013), because knowledge of its dependence on oxygen fugacity can aid in the understanding of point defect chemistry. Compositionally zoned crystals of orthopyroxene are common in meteorites, mantle rocks, lower crustal rocks and a variety of plutonic and volcanic igneous rocks. However, experimental difficulties have precluded direct determination of Fe-Mg diffusion rates in orthopyroxenes so far and the available information comes from (1) Mg tracer diffusion coefficients obtained from isotope tracer studies using enriched ^{25}MgO films (Schwandt et al. 1998), (2) calculations of interdiffusion rates based on the (diffusion-controlled) order-disorder kinetics measured in orthopyroxene (Ganguly and Tazzoli, 1994), and (3) indirect estimates from the comparison of diffusion widths in coexisting garnets and olivines, in which Fe-Mg diffusion rates are relatively well known (e.g., Smith and Barron, 1991; Klügel 2001).

In this study, we directly measured Fe-Mg interdiffusion coefficients parallel to the three main crystallographic axes between 870 and 1100 °C in two natural orthopyroxene single crystals under atmospheric pressure and between controlled oxygen fugacity of 10^{-11} and 10^{-7} Pa using a

rigorously tested experimental method that enables accurate determination of diffusion coefficients within the range of 10^{-19} - 10^{-21} m^2/s. The method uses pulsed laser ablation to deposit silicate thin films on oriented single crystals (of orthopyroxene in this case) and Rutherford Backscattering Spectroscopy (RBS) to measure film thicknesses and extract Fe concentration depth profiles. The general approach is identical to that of Mueller et al. (2013) for the measurement of Fe-Mg interdiffusion in clinopyroxene.

Experimental methods

Sample preparation and diffusion anneals

We used gem quality single crystals of brown and yellow orthopyroxene from Tanzania (referred to as OPX7 and OPX8 hereafter) in the diffusion experiments. The crystals are close to Fe-Mg solid solutions that differ in composition, mainly in the mole fraction of the ferrosilite component, Fs_1 and Fs_9 in Opx8 and Opx7, respectively (Table 1). The crystals were oriented optically using idiomorphic crystal faces and cleavage planes and a spindle stage setup attached to a computer, cut perpendicular to mostly the [001] axis (space group: Pbca) and in a few cases (OPX7 crystals) to [010] or [100] axis. The crystals were polished mechanically using diamond compounds with a final chemical-mechanical polishing step using colloidal silica compounds. We applied the same polishing procedure as for the olivine single crystals from our earlier studies (e.g., Chakraborty 1997, Dohmen et al. 2007). The orientation of the polished crystals was checked using electron backscatter diffraction in a SEM. Orthopyroxene slices of about 1.5 mm thickness were cut into smaller pieces with a polished surface of at least 4 mm^2. The polished crystals are clear and transparent with some occasional small cracks, mainly along cleavage planes. In the diffusion experiments, only samples that had an optically crack-free area of at least 3 mm^2 near the center of the sample were used. The polished crystals were coated with a silicate

thin film by pulsed laser ablation of a synthetic polycrystalline olivine pellet with composition of $Fo_{30}Fa_{70}$ (Dohmen et al. 2002, 2007). The Fe-rich thin films serve as the diffusion reservoir to exchange Fe and Mg with the orthopyroxene single crystals. For the equilibrium compositions of coexisting olivine and orthopyroxene, the mole fraction of the fayalite component in olivine is approximately equal to the mole fraction of the ferrosilite component in orthopyroxene (i.e., $X_{Fe}^{ol} \approx X_{Fe}^{opx}$) (Von Seckendorff and O'Neill 1993). Therefore, an olivine thin film with X_{Fe}^{ol} much higher than 0.1 results in a strong gradient in chemical potential between the film and the crystal that drives a diffusive flux of Fe into, and Mg out of, the orthopyroxene crystal. Furthermore, trials with various other compositions of thin films revealed that the chosen composition was ideally non-reactive, i.e., no other phases were produced by net-transfer reactions between the film and orthopyroxene crystals during the diffusion anneal. Following the procedure of our earlier experiments (Dohmen et al. 2002, Dohmen et al. 2007, Mueller et al. 2013) we obtain amorphous thin films with a roughness on the order of a nm and a homogeneous thickness (+/-10%) over the area of our orthopyroxene crystals. We used an excimer laser (LPX305i) to produce laser pulses with a wavelength of 193 nm at a frequency of 10 Hz. Laser fluences were between 1-5 J/cm^2, which yielded typically a film thickness of about 50 nm after 10 minutes. Before the deposition, the orthopyroxene single crystals were heated within the deposition chamber under vacuum at about 10^{-3} Pa (for details of the setup, see Dohmen et al. 2002) up to 400 °C for 15 minutes to remove volatile absorbants on the surface, in particular H_2O. The deposition was carried out approximately at room temperature and a background gas pressure of around 10^{-4} Pa. In most cases we deposited 2-4 samples simultaneously of which we kept one sample as a reference sample to determine the initial film thickness and composition before the diffusion anneal. We annealed the thin film/single crystal diffusion couples in high temperature furnaces at atmospheric pressure with the oxygen fugacity controlled by a flowing

gas mixture of CO and CO_2 (see also Dohmen et al. 2007). The experimental condition of each run is given in Table 2. In each run, we simultaneously annealed Opx7 and Opx8 crystals coated with a thin film, thus providing a direct comparison of the rate of Fe-Mg interdiffusion in orthopyroxene crystals with two different major element compositions.

Sample characterization and diffusion profile measurement

Thin film coated samples, annealed and not annealed, were investigated using a variety of methods to characterize the surface topography, the thin film geometry and composition: reflected light microscopy, high resolution thermally aided Field Emission Scanning Electron Microscopy (LEO, Zeiss, 1530 Gemini FESEM), white light interference microscopy, and Rutherford Backscattering Spectroscopy (RBS). In addition we used RBS to measure the concentration of Fe as a function of depth measured from the surface of the sample (for details of the principle see for example Dohmen et al. 2002, Dohmen et al. 2007, Cherniak et al. 2010). The RBS analyses were carried out at the RUBION facility of the Ruhr-University Bochum using a 4 MeV Tandem accelerator which is used to generate a beam of α-particles at 2 MeV that is focused onto the sample. Measurements were done with a final aperture of 0.5 mm to enable analysis of small samples, a beam current typically between 20 and 50 nA, a detecting angle of 160° with a silicon particle detector at an energy resolution of about 16-20 keV, and the sample surface tilted at 7° relative to the beam direction to avoid channeling. RBS spectra are fitted by an iterative procedure using the software RBX (Version 5.18, Kotai 1994) for spectra simulation, and Fe concentration depth profiles were extracted from the RBS spectra (see also Dohmen et al. 2007).

Results

General observations: Thin film morphology and composition

Investigation of the annealed thin film diffusion couples clearly show that the films served as an ideal diffusion reservoir and diffusion profiles can be extracted from these samples using RBS. Analysis of RBS spectra of reference samples (Fig. 1) revealed that the olivine thin films typically exhibited a thickness between 20 and 90 nm, a ratio of Fe/(Fe+Mg) between 0.66 and 0.83, and a significant excess in Si ($1.07 < (Fe+Mg)/Si < 1.47$) compared to an ideal olivine stoichiometry. As shown in earlier studies the films are amorphous after deposition at room temperature (Dohmen et al. 2002; Milke et al. 2007; Marquardt et al. 2010). During the diffusion anneal the films, at least partially, crystallized to a compact polycrystalline matrix with grain size, grain shape, distribution of grains, and possibly degree of crystallization depending on initial film properties and annealing conditions. Detailed inspection of the films using optical and electron microscopy revealed that the samples exhibited regular surfaces with no evidence for significant topography or de-wetting of the films (Fig. 2). The roughness of the surface as measured with the phase-shift interference light microscope is typically below 10 nm; thus, considerable convolution effects are not expected for the depth profile analysis with RBS. In fact, a steeper gradient of the Fe signal at the expected position of the layer-substrate interface still allows the layer to be identified in the RBS spectra. In all cases, the RBS spectra of the diffusion couples show that after initial rapid crystallization the film behaves as a stable layer of finite thickness, maintaining a gradient in the Fe-Mg exchange chemical potential to drive a diffusive flux of Fe into the orthopyroxene crystal (e.g. Fig. 1). Due to the excess in Si compared to olivine, we can expect that after complete re-crystallization the layer should form a mixture of olivine and orthopyroxene, which during the anneal progressively exchanges Fe and Mg with the single

crystal. The excess silica also serves here as a buffer for the activity of silica, which may affect diffusion in silicates (e.g, Zhukova et al. 2014). Consequently, the RBS spectra of the annealed samples were simulated with the following sequence of layers: (i) A layer with a (Fe+Mg)/Si ratio as observed in the reference sample but with different Fe/(Fe+Mg) ratio. (ii) A multi-layer with opx stoichiometry and a progressively decreasing Fe/(Fe+Mg) ratio described by an error function. Each layer has a thickness of 10 nm and the total number of layers depends on the length of the diffusion profile. (iii) An infinite substrate with a composition as given by the microprobe analysis. With such a set of layers we were able to fit the RBS spectra of annealed samples in all cases within the uncertainty given by the counting statistics of the alpha particles. The main exception is that for the simulation of the RBS spectra of the Opx8 samples (even the reference samples) we used a higher Fe content than that inferred from the microprobe analysis - this is related to mainly Ca and to a minor degree to Mn (Table 1) that contribute to a background signal in the RBS spectrum. From the RBS spectra we do not have any indication of a reaction between the layer and the substrate or of strong convolution effects because of a non-ideal thin film geometry. The proper simulation of the RBS spectra is a prerequisite for the extraction of an accurate Fe concentration depth profile since the Fe content varying with depth strongly influences the stopping power of the alpha particles, which affects in turn the de-convolution of the RBS spectra and calculation of the depth scale (e.g., Kotai, 1994).

Characteristics of the Fe concentration depth profiles and fitting procedure

From the fitting of the Fe concentration depth profiles we have determined $D_{\text{Fe-Mg}}$ for the two types of orthopyroxene single crystals and also tried to obtain a constraint on the dependence of $D_{\text{Fe-Mg}}$ on X_{Fe} from the profile shapes. The extracted Fe concentration-depth profiles have several significant features (e.g., Fig. 1b): (i) The composition within the film is roughly homogeneous, which indicates significantly faster Fe-Mg diffusion within the layer compared to the substrate.

This observation is consistent with the polycrystalline nature of the film and the presence of olivine, since Fe-Mg diffusion in olivine is expected to be much faster than in orthopyroxene. (ii) We can sometimes identify an abrupt change in the Fe concentration at the thin film/substrate interface, which is only possible if concentrations from the layer and the crystal are well separated in the depth profile. In turn, this indicates a constant layer thickness (+/-5 nm) across the area of incidence of the alpha particle beam. Since the layer has a larger (Fe+Mg)/Si ratio than the orthopyroxene single crystal, even for local equilibrium of the Fe/(Fe+Mg) ratio at the thin film/substrate interface we would obtain a discontinuity for the concentration of Fe (expressed as atomic fraction) at this interface. This abrupt change can be considered in the simulation by simply defining a partition coefficient for Fe between the bulk film composed of an olivine/orthopyroxene mixture and the orthopyroxene crystal. (iii) The concentration profile in the region of the single crystal shows a typical profile shape for a diffusion profile.

The extracted Fe concentration-depth profiles were fitted by solving the appropriate diffusion equation. For an ideal thin film geometry, the temporal evolution of the concentration-depth profile of Fe can be described by a one-dimensional diffusion equation where the thin film and the orthopyroxene crystal are treated as separate diffusion media with different Fe-Mg interdiffusion coefficients. We assume a zero flux boundary condition at the surface of the crystal and mass balance as well as local equilibrium at the thin film/crystal interface (for the set of equations, see, for example, Eqns. 1-4 in Watson and Dohmen 2010). An analytical solution is available for the case of constant diffusion coefficients in each media, as given in Watson and Dohmen (2010). However, Fe-Mg diffusion in olivine is strongly dependent on the mole fraction of the Fe end-member, which can be identified by the detailed profile shape (Chakraborty 1997, Dohmen et al. 2007). Therefore we considered the possibility of such a compositional dependence and used a numerical method for fitting, and in analogy to olivine, used

$D(X_{Fe}) = D^{\circ} \cdot 10^{mX_{Fe}}$, where D° and m are fitting parameters, as the relation to describe this dependence. The initial concentration in the film and the crystal as well as the thickness of the thin film were determined from RBS measurements of the simultaneously deposited unannealed reference samples. The two concentrations, and the thickness with some tolerance, were considered to be known inputs in the fitting procedure. In combination, these provide a mass balance constraint as well for the fitting procedure - the missing Fe from the film had to diffuse into the crystal. To find the best fit we applied a simplified regression procedure. We solved the one dimensional diffusion equation numerically using a finite difference scheme with D° and m as free parameters. For a given m, we varied the diffusion coefficient D° by steps of 0.05 log units and calculated the summed squares of the residuals, χ^2 to find a D° with minimum χ^2. The values for D° and m are correlated (see also Dohmen et al. 2007). It is typically possible to obtain fits to the profiles with similar values for χ^2 but rather different values for m and hence D°. Therefore, given the shapes of the experimentally measured profiles, the fitting procedure is not very sensitive for determining m and we varied this parameter only between the values of 0 – 3 in steps of 1. For most profiles, values of m = 1 or m = 2 gave the best fit. To avoid artificial variation of the diffusion coefficients because of these correlation effects we fixed the value of m to 1 and report values for the initial single crystal composition (X_{Fe} = 0.09 for Opx7 and X_{Fe} = 0.01 for Opx8). For a fixed value of m, the individual error of the diffusion coefficient as determined by the regression procedure is typically within 0.1 log units (Table 2). The total error is higher because of the correlations of D° and m, as well as because of systematic errors introduced during sample preparation or during the extraction of concentration profiles using RBX from the spectra (e.g., the depth scale relates directly to the uncertainty in the stopping power used by the program RBX, which for chemical compounds could differ by 10-20 %, Ziegler and Manoyan, 1988); Faak et al. (2013) discuss various possible sources of errors in the

determination of diffusion coefficients. Reproducibility and time series experiments indicate overall uncertainties of ± 0.2 log units (e.g., Fig. 3). The final extracted values for $D_{\text{Fe-Mg}}$ are reported in Table 2 and displayed in an Arrhenius diagram (Fig. 4a and b). Irrespective of the assumed compositional dependence the diffusion coefficient obtained for Opx7 is typically larger than that for Opx8 from the same experiment. On average, $D_{\text{Fe-Mg}}$ for Opx7 is a factor of 2 faster than for Opx8. This would imply an exponent *m* of ~3 if this difference is solely related to the different ferrosilite contents of the two crystals and not to different trace or minor element contents.

Effect of temperature and fO_2

The diffusion coefficients measured parallel to the c-axis for Opx 7 at the nominal log (fO_2 [Pa]) = -11 and -7 appear to be shifted by a constant value in an Arrhenius plot indicating a constant activation energy and an effect of fO_2 (Fig. 4a). Therefore, we fitted these data for Opx7 using the measured fO_2 with the following relationship

$$\log D^{c}_{\text{Fe-Mg}} = \log D_0 - Q/\{\ln(10)RT\} + n \log fO_2, \qquad (1)$$

where Q = 308 ± 23 kJ/mol, log (D_0 [m^2/s]) = -5.95 ± 0.83, and n = 0.053 ± 0.027.

Unlike for Opx7, we cannot identify any significant effect of fO_2 for the diffusion data from Opx8 (Fig. 4b) and these data can be well reproduced by a single Arrhenius relationship with log (D_0 [m^2/s]) = -3.78 ± 1.26 and Q = 377 ± 30 kJ/mol.

Diffusion anisotropy

The diffusion experiments performed with Opx7 oriented parallel to the a-axis clearly demonstrate that Fe-Mg diffusion is slower along these directions compared to diffusion parallel to the c-axis (Fig. 4a). Considering also the sparse data for the b-axis, we can conclude that

$D^{c}_{\text{Fe-Mg}} \geq D^{b}_{\text{Fe-Mg}} > D^{a}_{\text{Fe-Mg}}$. The observed diffusion anisotropy is consistent with basic crystallographic considerations of Ganguly and Tazzoli (1994) for diffusion of octahedral cations in orthopyroxene. From a weighted linear regression of the data for $D^{a}_{\text{Fe-Mg}}$ in the Arrhenius plot we obtain an activation energy of 299 ± 65 kJ/mol, which is the same within the error as those for $D^{c}_{\text{Fe-Mg}}$ (Eqn. 1). Since the activation energy for $D^{c}_{\text{Fe-Mg}}$ is much better constrained and there is no clear indication of a different activation energy for $D^{a}_{\text{Fe-Mg}}$, we performed an additional linear regression of $D^{a}_{\text{Fe-Mg}}$ by fixing the activation energy to obtain a pre-exponential factor that is consistent with Eqn. 1, log (D_0 [m^2/s]) = -6.46 ± 0.09. We finally conclude that $D^{a}_{\text{Fe-Mg}}$ is slower by a factor of 3.5 than $D^{c}_{\text{Fe-Mg}}$ at all temperatures, at least within the temperature range of the experiments.

Discussion

Comparison with other estimates for Fe-Mg-diffusion in orthopyroxene

The only data set of directly measured diffusion coefficients that serves as an independent constraint for the present data set is from Schwandt et al. (1998) for Mg tracer diffusion in orthopyroxene of composition Fs_{11}. This data set comprises of four diffusion experiments at fO_2 = IW where three crystals were annealed simultaneously to measure diffusion parallel to the a-, b- and c-axis in order to fully constrain the diffusion tensor for the orthorhombic crystal. We observe two aspects from this data set (Fig. 5): (i) The quality of the data does not permit a clear resolution of any diffusion anisotropy for Mg; (ii) The data are very similar to diffusion coefficients predicted using Equation 1 (based on our data for $D_{Fe\text{-}Mg}$) at fO_2 = IW. The tracer diffusion coefficient of Mg is related to $D_{Fe\text{-}Mg}$ according to the following equation, as derived for example by Barrer et al. (1963) or Lasaga (1979) for interdiffusion in binary ionic solutions

$$D_{Fe-Mg} = \frac{D^*_{\mathrm{Mg}} \cdot D^*_{\mathrm{Fe}}}{X_{\mathrm{Mg}} D^*_{\mathrm{Mg}} + X_{\mathrm{Fe}} D^*_{\mathrm{Fe}}} \cdot \left(1 + \frac{\partial \ln \gamma_{\mathrm{Fs}}}{\partial \ln X_{\mathrm{Fe}}}\right) \qquad (2)$$

where D_i^* is the tracer diffusion coefficient of i at the composition of interest, X_{Mg} is the mole fraction of Mg and γ_{Fe} is the activity coefficient of the Fe-component of orthopyroxene. It is reasonable to assume a nearly ideal solid solution behavior for orthopyroxene (Von Seckendorff and O'Neill, 1993) such that the activity coefficient term is unity. If $D_{\mathrm{Fe}}^* \approx D_{\mathrm{Mg}}^*$, as it was shown for FeMg-rich garnets (Ganguly et al., 1998; Borinski et al., 2012), olivine (Chakraborty et al., 1994; Hermeling and Schmalzried, 1984), and spinel (Liermann and Ganguly, 2002; Vogt et al. 2015), then for $X_{\mathrm{Fe}} = 0.11$ it can be shown numerically that $D_{\mathrm{Mg}}^* \leq D_{\mathrm{Fe\text{-}Mg}} \leq 10\ D_{\mathrm{Mg}}^*$ (see Fig. 2 in Vogt et al. 2015), irrespective of the value of D_{Fe}^*. Consistent with this expectation, we

find that at around 900 °C, where both $D_{\text{Fe-Mg}}$ and D_{Mg}* were measured at similar fO_2 (note that log fO_2 in Pa of the IW buffer is -11.72 at 900 °C), these diffusion coefficients are almost indistinguishable considering the reproducibility of diffusion coefficient measurements.

Also shown in Figure 5 is the estimate for $D_{\text{Fe-Mg}}$ of Ganguly and Tazzoli (1994) for $X_{\text{Fe}} = 0.11$. This was inferred from the rates of order-disorder kinetics of Fe and Mg between the M1 and M2 sites in orthopyroxene that were measured experimentally in the temperature range of 500 – 800 °C at an fO_2 at, or close to, IW. For modeling of Fe-Mg zoning in orthopyroxene phenocrysts, Allan et al. (2013) considered an additional fO_2 dependence to derive the following more general expression from Ganguly and Tazzoli (1994):

$$\log D_{\text{Fe-Mg}}\left[\text{m}^2/\text{s}\right] = -9.54 + 2.6 \cdot X_{\text{Fe}} - \frac{12,530}{T[K]} + \frac{1}{6} \cdot \log\left(\frac{fO_2(\text{sample},T)}{fO_2(\text{IW},T)}\right) \quad (3)$$

The fO_2 exponent of 1/6 was based on a simplified point defect model for olivine, which is generally applied to other Fe-bearing minerals (e.g, garnet: Chakraborty and Ganguly, 1992), where vacancies are considered to form on the metal site by partial oxidation of Fe^{2+} to Fe^{3+}. Furthermore Stimpfl et al. (2005) inferred the same fO_2 exponent from the ordering kinetics of Fe-Mg during a cooling experiment with Opx of Fs_{50} content. However, such a fO_2 dependence has never been verified experimentally for orthopyroxene with lower Fs contents and appears to overestimate this dependence when compared to our experimental results. We used Equation 3 to calculate $D_{\text{Fe-Mg}}$ at our experimental run conditions (log fO_2 (Pa) = -11, $X_{\text{Fe}} = 0.11$) and at relatively oxidizing conditions (fO_2 (Pa) = NNO). We find that the calculated $D_{\text{Fe-Mg}}$ are significantly higher than that measured at $T \leq 900$ °C (Fig. 5 and inset in Fig. 5). The fO_2 correction term in Equation 3 has two effects: (i) in comparison to the expression of Ganguly and Tazzoli (1994) the calculated $D_{\text{Fe-Mg}}$ is much larger because log fO_2 (Pa) = -11 is significantly higher than fO_2 = IW for T < 900 °C (e.g., log fO_2 (Pa) = -13.9 at 800 °C). (ii) For a constant log

fO_2 the activation energy becomes significantly smaller (150 kJ/mol, see inset in Fig. 5) compared to the apparent activation energy along a fO_2 buffer. For example, for fO_2 = IW, Ganguly and Tazzoli (1994) estimated an apparent activation energy of 240±8 kJ/mol. The low activation energy of 150 kJ/mol is in strong contradiction to our experimentally observed activation energy at constant fO_2 (308±23 kJ/mol). If the fO_2 dependence determined by us is used, the apparent activation energy for fO_2 variation along the IW buffer is higher than the true activation energy at constant fO_2 by only about 30 kJ/mol (≈336 kJ/mol). In fact, the estimate for $D_{Fe\text{-}Mg}$ of Ganguly and Tazzoli (1994), when extrapolated to the temperature range of the present study without considering any fO_2 dependence, appears to be very consistent with our dataset at log fO_2 (Pa) = -11. These observations strongly indicate that for orthopyroxene, at least with Fs contents of around 10 mol %, there is only a minor fO_2 dependence of the diffusion coefficients. Finally, based on the consistency with the data of Schwandt et al. (1998), we conclude that Eqn. 3 represents a robust Arrhenius equation for the temperature range 750 – 1100 °C. Experiments on the order/disorder kinetics suggest that (i) for T < 750 °C Fe-Mg diffusion in Opx has a smaller activation energy and (ii) for Opx with higher Fs contents, diffusion rates could be more sensitive to fO_2. These open issues may need additional experiments in the future but in the section below, the order/disorder experiments are discussed in more detail.

Diffusion mechanisms

In olivine, an absence of fO_2 dependence for Fe-Mg interdiffusion was observed below a critical oxygen fugacity and temperature (Dohmen et al. 2007). This behavior was explained by a quantitative point defect model (Dohmen and Chakraborty 2007). In this model, vacancies in the octahedral metal sites are charge balanced by trivalent cations – some of which may be aliovalent

impurities such as Cr^{3+} or Al^{3+}, while the rest is Fe^{3+} produced by the oxidation of Fe^{2+}. The concentration of Fe^{3+} is sensitive to ambient fO_2, but the concentrations of elements like Al^{3+} are not. Therefore, with decreasing fO_2 (and temperature, or Fe content of olivine) as the concentration of Fe^{3+} decreases, so does the concentration of vacancies that are charge balanced by it, and at some point vacancies charge balanced by other trivalent cations such as Al^{3+} become dominant. At this point, diffusion coefficients cease to be dependent on fO_2. This behavior has been described as a transition in diffusion mechanism from a fO_2-dependent transition metal extrinsic diffusion (TaMED) to a fO_2-independent pure extrinsic diffusion (PED) (Chakraborty, 1997). The transition point depends on fO_2, temperature, and the composition (i.e. Fe content as well as the concentration of trivalent trace elements) of the olivine.

In pyroxenes, trivalent cations in octahedral positions are much more abundant (e.g. octahedral Al) and consequently, such larger variations in the fO_2-dependence of diffusion coefficients are expected. Indeed, this effect has already been found for clinopyroxenes (Müller et al., 2013). Such a shift from a TaMED to a PED mechanism in orthopyroxene is supported by the data set for Opx8 with $X_{Fe} = 0.01$. No effect of fO_2 on diffusion coefficients is observed in this pyroxene in the experimentally investigated range of fO_2 and T. In addition, the activation energy of diffusion is significantly higher in Opx8 compared to that in Opx7. The difference in activation energy and dependence on fO_2 of diffusion coefficients between these two pyroxene compositions indicate that diffusion occurs by different mechanisms in these two crystals: TaMED in Opx7 vs. PED in Opx8. In fact the effect of fO_2 on $D_{Fe\text{-}Mg}$ in Opx7 is much smaller than would be expected from simplified point defect models (exponent n in Eq. (1): 1/20 vs. 1/6) and hence we may speculate here that for Fs_9 the experimental conditions were at the transition between TaMED and PED. It is expected that at a given fO_2, the Fe^{3+} content of pyroxenes with

lower Fe contents would be correspondingly lower, and hence the transition from TaMED to PED regime would be shifted to even higher fO_2 and higher temperatures. The same effect would be obtained for pyroxenes with similar Fe contents, but higher concentrations of trivalent cations in the octahedral site. Therefore, besides the fO_2, the detailed composition of orthopyroxene (major and to some extent also minor elements) also has an effect on $D_{Fe\text{-}Mg}$. This discussion implies that data from Opx7 and Opx8 cannot be combined to derive a general expression for the effect of X_{Fe} on $D_{Fe\text{-}Mg}$ because diffusion in the two crystals occurred by different mechanisms at the experimental conditions. Nevertheless, it was shown in the results section that the profile shapes in each crystal also indicate a positive dependence of $D_{Fe\text{-}Mg}$ on X_{Fe}, although we were unable to quantify this dependence. We can conclude therefore that for increasing ferrosilite content in opx, $D_{Fe\text{-}Mg}$ appears to be faster, in general agreement with the expression of Ganguly and Tazzoli (1994) and Equation 3.

Fe-Mg diffusion in orthopyroxene and the connection to order-disorder kinetics

To evaluate the reliability of the compositional and fO_2 dependence in Equation 3 (the exponent 2.6), we revisited the order-disorder rates used by Ganguly and Tazzoli (1994) to derive $D_{Fe\text{-}Mg}$, and included the recalculated data of Kroll et al. (1997) and the more recent dataset of Stimpfl et al. (2005) in the considerations. The order-disorder rates in orthopyroxene can be characterized by a reaction rate constant, K^+, which is typically determined by isothermal annealing of an orthopyroxene crystal and subsequent measurement of the ordering state using single crystal X-ray diffraction or Mössbauer spectroscopy. Measured rate constants from isothermal experiments at fO_2 mostly at, or within one log unit, of IW by Besancon (1981), Anovitz et al. (1988), Saxena et al. (1987, 1989), Skogby (1992), Schlenz (1995), Kroll et al. (1997) and Stimpfl et al. (2005)

are summarized in Figure 6 for orthopyroxenes of various Fe-contents (X_{Fe}). In addition, we show rate constants that were extracted from a cooling experiment by Stimpfl et al. (2005). There has been considerable discussion in the literature about the merits and demerits of different analytical methods (e.g., X-ray diffraction vs. Mössbauer spectroscopy), data reduction procedures, and sample preparation techniques (see Stimpfl et al., 2005; Wang et al., 2005; Kroll et al., 1997). Therefore, it is difficult to evaluate the exact uncertainties in K^+ obtained from different studies. However, comparison of data from the various sources in Figure 6 reveal that all the data form a cluster (gray area in Fig. 6), with only two sets that deviate substantially from the others: Anovitz et al. (1988) and those from the non-isothermal, cooling experiments of Stimpfl et al. (2005). Kroll et al. (1997) recalculated rate constants from the raw data of the ordering parameters as a function of time from the different experimental studies using a consistent modeling approach. The ordering rates obtained from the data of Anovitz et al. (1988) using this calculation scheme are significantly different from those reported by Anovitz et al. (1988); for other studies (e.g., Besancon 1981 or Saxena et al. 1987) the original and the recalculated rates were similar. Therefore, in Fig. 6 we have also shown the data from Anovitz et al. (1988) as calculated by Kroll et al. (1997). It should be noted here that the compositional dependence of diffusion rates obtained by Ganguly and Tazzoli (1994) was mainly based on the data of Anovitz et al. (1989). In Kroll et al. (1997) a global fit of the re-determined rate constants was given that does not explicitly depend on fO_2 and indicates a much smaller compositional dependence of K^+ than those of Ganguly and Tazzoli (1994); this is also illustrated in Fig. 6. Thus, once the recalculated values of Kroll et al. (1997) are considered the only remaining dataset that deviates substantially from the rest (gray area in Fig. 6) is that from the cooling experiment of Stimpfl et al. (2005).

Rather than calculate diffusion coefficients from order-disorder kinetic rates showing such scatter and uncertainty, we have taken the alternate approach of calculating rate-constants from our measured diffusion data and comparing these with all of the experimental results for order-disorder kinetics plotted in Fig. 6. To do this, we assume that the equation derived by Ganguly and Tazzoli (1994) is valid. According to them, the reaction rate constant K^+ is related to the diffusion coefficient $D_{\text{Fe-Mg}}$ by

$$D_{\text{Fe-Mg}} \approx \frac{\lambda^2 K^+}{2} \cdot \left(1 + \frac{1}{K_D}\right) \tag{4}$$

where λ is the average jump distance between neighboring M1 and M2 sites in orthopyroxene and K_D is the distribution coefficient of Fe and Mg between the M1 and M2 sites at thermodynamic equilibrium. It has been shown (Wang et al., 2005) that K_D is insensitive to X_{Fe} and can be parameterized by:

$$\ln K_D = 0.391 - \frac{2205}{T[K]} \tag{5}$$

Thus, according to Equation 4, any dependence of K^+ on X_{Fe} can be directly transferred to a dependence of $D_{\text{Fe-Mg}}$ on X_{Fe}, and vice versa. It should also be noted that the temperature dependence of K_D and its uncertainty are much smaller compared to the activation energy of the diffusion coefficient and thus the temperature dependence of K^+ should closely correspond to the activation energy of $D_{\text{Fe-Mg}}$. We have used $D_{\text{Fe-Mg}}$ as given by equation 1 for fO_2 = IW in a re-casted form of Equation 4 to calculate K^+– this calculated trend is shown in Figure 6 as a solid line. Even though Equation 4 is a relatively simplistic approach, we obtain a remarkable match between the experimental data for K^+ and K^+ calculated from $D_{\text{Fe-Mg}}$ at temperatures around 900 °C where an overlap exists between measured diffusion coefficients and rate constants. As noted above, the overall pattern of all available data for K^+ taken together suggests that the rate-

constant increases with the Fe-content of orthopyroxene, but that this dependence is much smaller than that indicated by Eqn. 3. By implication, $D_{\text{Fe-Mg}}$, at least for orthopyroxenes with Fs-contents < 50 mole percent, should also have a weak compositional dependence. The compositional dependence with an exponent m = 1 that we used for fitting the experimental diffusion profiles is very consistent with the variation of K^+ with Fs-content (Figure 6). Therefore to calculate $D_{\text{Fe-Mg}}$ for molar fractions of Fe in the range of 0.09-0.5 we recommend the use of $D\left(X_{Fe}, T, fO_2\right) = D(T, fO_2) \cdot 10^{m(X_{Fe}-0.09)}$ with m = 1 and $D(T, fO_2)$ calculated according to Equation 1.

The comparison of rate constants calculated from diffusion coefficients with directly measured rate constants at temperatures lower than 900 °C indicates that the apparent activation energy for K^+ calculated from $D_{Fe\text{-}Mg}$ at fO_2 = IW is higher than that suggested by the trend of the measured data. However, as discussed above, we have observed only a small effect of fO_2 on $D_{Fe\text{-}Mg}$ and it is quite likely that K^+ and $D_{\text{Fe-Mg}}$ even become independent of fO_2 at these relatively reducing and low temperature conditions. If that is the case, then the slope of the line calculated from the diffusion data would be more similar to the trend of the measured data on order-disorder kinetics. This aspect may be clarified when diffusion coefficients measured directly at lower temperatures become available in the future.

Comparison with other diffusion data for orthopyroxene, and Fe-Mg diffusion in other related minerals

In Figure 7 we compare $D_{\text{Fe-Mg}}$ with diffusion of other cations in orthopyroxene. As observed in many other minerals (e.g., Brady and Cherniak, 2010), it is obvious that diffusion of divalent

cations is significantly faster than diffusion of trivalent cations (Cr^{3+}, Nd^{3+}, Gd^{3+}) or quadrivalent cations (Ti^{4+}). Furthermore, there seems to be the general trend that diffusion of smaller ions is faster than larger ions of the same valence (e.g., Mg^{2+} vs. Pb^{2+}, Cr^{3+} vs. Nd^{3+}) with activation energies ranging between 250 kJ/mol and 380 kJ/mol. A number of studies investigated diffusion only parallel to [210] direction but Cr diffusion (Ganguly et al. 2007) and Nd diffusion (Sano et al. 2011) is faster //c by up to one order of magnitude compared to diffusion //a or //b, which is similar to the behavior found here for $D_{Fe\text{-}Mg}$. The diffusion mechanism of Nd cannot be directly compared to those of Fe-Mg since it occupies exclusively the M2 site and therefore has likely a different jump path in orthopyroxene (see the discussion in Sano et al. 2011 on the explanation for the observed anisotropy for Nd). The diffusion anisotropy of Cr follows the same sequence as $D_{Fe\text{-}Mg}$ with D //c > D //b > D //a but appears to be slightly larger. The effect of fO_2 on diffusion of cations occupying the M sites in orthopyroxene seems to be variable. Sano et al. (2011) and Ganguly et al. (2007) found a negative effect of fO_2 on D_{Cr} and D_{Nd}, whereas some studies did not find any effect of fO_2 for D_{Nd}, and other REE (Cherniak and Liang 2007) or D_{Ti} (Cherniak and Liang 2012). Only for Pb a significant positive dependence of diffusivity on fO_2 was found (Cherniak 2001). This positive effect for Pb, with an exponent of n ranging from 0.14 to 0.2 in Equation 1 is about two times larger than the effect we found here for $D_{Fe\text{-}Mg}$. For further discussion of other experimental data see also Cherniak and Dimanov (2010).

Diffusion rates of Fe-Mg in orthopyroxene are similar to the rates of diffusion in garnets (Borinski et al., 2012), and are somewhat faster than the rates in clinopyroxenes (Müller et al., 2013). They are slower than the diffusion rates in olivines (Dohmen et al., 2007) and spinel (Liermann and Ganguly, 2002; Vogt et al., 2015) and the relationships are illustrated in Fig. 8.

Implications of the results of this study for diffusion chronometry and geothermometry

Our data implies that in most situations, diffusion in orthopyroxene would be the rate determining step for the closure of Fe-Mg based thermometers and chronometers; the only exception being situations where exchange is controlled by clinopyroxenes. In particular, the similarity in diffusion rates of Fe-Mg in garnets and orthopyroxenes provides an excellent tool to distinguish chemical zoning formed by diffusive exchange from those formed by other processes (e.g. crystal growth or resorption) – profile lengths should be very similar in coexisting garnets and orthopyroxenes when the zoning is formed by diffusive exchange but the diffusion anisotropy needs to be considered for orthopyroxene. This is consistent with observations in different mantle and metamorphic rocks (e.g. Smith and Barron, 1991; Pattison and Begin, 1994). Together, these minerals therefore form a robust chronometer for lower crustal metamorphic and mantle derived rocks.

In contrast, caution should be exercised in evaluating Fe-Mg partitioning data between orthopyroxenes and olivines or spinel. There may be situations where the compositions of olivines or spinels may be reset at lower temperatures by exchange between themselves or with a different phase that is present, while orthopyroxenes retain their compositions from a higher temperature segment of the thermal history. Such coexisting olivine – orthopyroxene or spinel – orthopyroxene pairs would be in disequilibrium and yield erroneous temperatures if their compositions are used in thermometric expressions. This is often the case in many meteorites (e.g. Seckendorff et al., 1992; Eisenhour et al., 1993) and equilibrium should be evaluated before interpreting temperatures obtained from coexisting pairs of these minerals.

Acknowledgements

This study was supported by funds from the Ruhr-Universität Bochum. Rutherford Backscattering spectroscopy was performed at and supported by RUBION, central unit of the Ruhr-Universita□t Bochum. We thank associate editor John Ferry for handling the manuscript and reviewers Daniele Cherniak and Jibamitra Ganguly for detailed and constructive comments that helped to improve the manuscript.

References

Allan, A.S.R., Morgan, D.J., Wilson, C.J.N., and Millet, M.-A. (2013) From mush to eruption in centuries: assembly of the super-sized Oruanui magma body. Contributions to Mineralogy and Petrology, 166, 143-164.

Anovitz, L.M., Essene, E.J., and Dunham, W.R. (1988) Order-disorder experiments on orthopyroxenes: implication for the orthopyroxene geospeedometer. American Mineralogist, 73, 1060-1073.

Barrer, R.M., Bartholomew, R.F., and Rees, L.V.C. (1963) Ion exchange in porous crystals. Part II. The relationship between self and exchange-diffusion coefficients. Journal of Physics and Chemistry of Solids, 24, 309-317.

Besancon, J.R. (1981) Rate of cation disordering in orthopyroxenes. American Mineralogist, 66, 965-973.

Borinski, S.A., Hoppe, U., Chakraborty, S., Ganguly, J., and Bhowmik, S.K. (2012) Multicomponent diffusion in garnets I: general theoretical considerations and experimental data for Fe-Mg systems. Contributions to Mineralogy and Petrology, 164, 571-586.

Brady, J.B., and Cherniak, D.J. (2010) Diffusion in minerals: an overview of published experimental data. Reviews in Mineralogy and Geochemistry, 72, 899-920.

Chamberlain, K.J., Morgan, D.J., and Wilson, C.J.N. (2014) Timescales of mixing and mobilisation in the Bishop Tuff magma body: perspectives from diffusion chronometry. Contributions to Mineralogy and Petrology, 168:1034, DOI 10.1007/s00410-014-1034-2.

Chakraborty, S., and Ganguly, J. (1992) Cation diffusion in aluminosilicate garnets: experimental determination in spessartine-almandine diffusion couples, evaluation of effective binary diffusion coefficients, and applications. Contributions to Mineralogy and Petrology, 111, 74-86.

Chakraborty, S., Farver, J.R., Yund, R.A., and Rubie, D.C. (1994) Mg tracer diffusion in synthetic forsterite and San Carlos olivine as a function of P, T, and fO_2. Physics and Chemistry of Minerals, 21, 489-500.

Chakraborty, S. (1997) Rates and mechanisms of Fe-Mg interdiffusion in olivine at 980°C–1300°C. Journal of Geophysical Research, 102, 12317-12331.

Cherniak, D.J. (2001) Pb diffusion in Cr diopside, augite, and enstatite, and consideration of the dependence of cation diffusion in pyroxene on oxygen fugacity. Chemical Geology, 177, 381-397.

Cherniak, D.J., and Liang, Y. (2012) Ti diffusion in natural pyroxene. Geochimica et Cosmochimica Acta, 98, 31-47.

Cherniak, D.J., and Liang, Y. (2007) Rare earth element diffusion in natural enstatite. Geochimica et Cosmochimica Acta, 71, 1324-1340.

Cherniak, D.J, Hervig, R., Koepke, J., Zhang, Y., and Zhao, D. (2010) Analytical Methods in Diffusion Studies. Reviews in Mineralogy and Geochemistry, 72, 107-169.

Cherniak, D.J., and Dimanov, A. (2010) Diffusion in Pyroxene, Mica and Amphibole. Reviews in Mineralogy and Geochemistry, 72, 641-690.

Dai, L., and Karato, S. (2009) Electrical conductivity of orthopyroxene: Implications for the water content of the asthenosphere. Proceedings of the Japan Academy, Ser. B, Physical and Biological Sciences, 85, 466-475.

Dodson, M.H. (1973) Closure temperature in cooling geochronological and petrological systems. Contributions to Mineralogy and Petrology, 40, 259-274.

Dodson, M.H. (1986) Closure profiles in cooling systems. In: Materials Science Forum, vol 7. Trans Tech Publications, Aedermannsdorf, Switzerland, 145-153.

Dohmen, R., and Chakraborty, S. (2007) Fe-Mg diffusion in olivine II: Point defect chemistry, diffusion mechanisms and a model for calculation of diffusion coefficients in natural olivine. Physics and Chemistry of Minerals, 34, 409-430.

Dohmen, R., Becker, H.-W., and Chakraborty, S. (2007) Fe–Mg diffusion in olivine I: experimental determination between 700 and 1,200 C as a function of composition, crystal orientation and oxygen fugacity. Physics and Chemistry of Minerals, 34, 389-407.

Dohmen, R., Becker, H.-W., Meissner, E., Etzel, T., and Chakraborty, S. (2002) Production of silicate thin films using pulsed laser deposition (PLD) and applications to studies in mineral kinetics. European Journal of Mineralogy, 14, 1155-1168.

Eisenhour, D.D., Buseck, P.R., Palme, H., and Zipfel, J. (1993) Micro-zoning in minerals of a Landes silicate inclusion. Abstract: Lunar and Planetary Science Conference, XXIV, 1220.

Faak, K., Chakraborty, S., and Coogan, L.A (2013) Mg in plagioclase: Experimental calibration of a new geothermometer and diffusion coefficients. Geochimica et Cosmochimica Acta, 123, 195-217.

Farla, R.J.M., Karato, S., and Cai, Z. (2013) Role of orthopyroxene in rheological weakening of the lithosphere via dynamic recrystallization. Proceedings of the National Academy of Sciences of the United States of America, 110, 16355-16360.

Ganguly, J., and Tazzoli, V. (1994) Fe^{2+}-Mg interdiffusion in orthopyroxene: Retrieval from the data on intracrystalline exchange reaction. American Mineralogist, 79, 930–937.

Ganguly, J., and Tirone, M. (1999) Diffusion closure temperature and age of a mineral with arbitrary extent of diffusion: theoretical formulation and applications. Earth and Planetary Science Letters, 170, 131-140.

Ganguly, J., Cheng, W., and Chakraborty, S. (1998) Cation diffusion in aluminosilicate garnets: experimental determination in pyrope- almandine diffusion couples. Contributions to Mineralogy and Petrology, 131, 171-180.

Ganguly, J., Ito, M., and Zhang, X. (2007) Cr diffusion in orthopyroxene; experimental determination, ^{53}Mn–^{53}Cr thermochronology, and planetary applications. Geochimica et Cosmochimica Acta, 71, 3915-3925.

Ganguly, J., Tirone, M., Chakraborty, S., and Domanik, K. (2013) H-chondrite parent asteroid: A multistage cooling, fragmentation and re-accretion history constrained by thermometric studies, diffusion kinetic modeling and geochronological data. Geochimica et Cosmochimica Acta, 105, 206-220.

Hermeling, J., and Schmalzried, H. (1984) Tracerdiffusion of the Fe-cations in Olivine $(Fe_xMg_{1-x})_2SiO_4$ (III). Physics and Chemistry of Minerals, 11, 161-166.

Kótai, E. (1994) Computer methods for analysis and simulation of RBS and ERDA spectra. Nuclear Instruments and Methods in Physics Research Section B: Beam Interactions with Materials and Atoms, 85, 588-596.

Klügel, A. (2001) Prolonged reactions between harzburgite xenoliths and silica-undersaturated melt: implications for dissolution and Fe-Mg interdiffusion rates of orthopyroxene. Contributions to Mineralogy and Petrology, 141, 1-14.

Kroll, H., Lueder, T., Schlenz, H., Kirfel, A., and Vad, T. (1997) The Fe^{2+}-Mg distribution in orthopyroxene: A critical assessment of its potential as a geospeedometer. European Journal of Mineralogy, 9, 705-733.

Lasaga, A.C. (1979) Multicomponent exchange and diffusion in silicates. Geochimica et Cosmochimica Acta, 43, 455-468.

Lasaga, A.C. (1983) Geospeedometry: An extension of geothermometry. In: Saxena SK (ed) Kinetics and equilibrium in mineral reactions, advances in physical geochemistry, Vol 3. Springer, Berlin Heidelberg New York Tokyo, 81-114.

Liermann, H.P., and Ganguly, J. (2002) Diffusion kinetics of Fe2+ and Mg in aluminous spinel: Experimental determination and applications. Geochimica et Cosmochimica Acta 66, 2903-2913.

Mackwell, S.J. (1991) High-temperature rheology of enstatite – implications for creep in the mantle. Geophysical Research Letters, 18, 2027-2030.

Marquardt, K., Petrishcheva, E., Abart, R., Gardés, E., Wirth, R., Dohmen, R., Becker, H.-W., and Heinrich, W. (2010) Volume diffusion of Ytterbium in YAG: thin-film experiments and combined TEM–RBS analysis. Physics and Chemistry of Minerals, 37, 751-760.

Milke, R., Dohmen, R., Becker, H.-W., and Wirth, R. (2007) Growth kinetics of enstatite reaction rims studied on nano scale, Part I: Methodology, microscopic observations and the role of water. Contributions to Mineralogy and Petrology, 154, 519-533.

Müller, T., Dohmen, R., Becker, H.-W., ter Heege, J.H., and Chakraborty, S. (2013) Fe-Mg interdiffusion rates in clinopyroxene: experimental data and implications for Fe-Mg exchange geothermometers. Contributions to Mineralogy and Petrology, 166, 1563-1576.

Pattison, D.R.M., and Begin, N.J. (1994) Zoning patterns in ortho-pyroxene and garnet in granulites – implications for geothermometry. Journal of Metamorphic Geology, 12, 387-410.

Rietmeijer, F.J.M., and Champness, P.E. (1982) Exsolution structures in calcic pyroxenes from the Bjerkreim-Skondal lopolith, SW Norway. Mineralogical Magazine, 45, 11-24.

Sano, J., Ganguly, J., Hervig, R., Dohmen, R., and Zhang, X. (2011) Neodymium diffusion in orthopyroxene: experimental studies and applications to geological and planetary problems. Geochimica et Cosmochimica Acta, 75, 4684-4698.

Saunders, K., Blundy, J., Dohmen, R., and Cashman, K. (2012) Linking petrology and seismology at an active volcano. Science, 336, 1023-1027.

Saxena, S.K., Tazzoli, V., Domeneghetti, M.C. (1987): Kinetics of Fe^{2+} -Mg distribution in aluminous orthopyroxenes. Physics and Chemistry of Minerals, 15, 140-147.

Saxena, S.K., Domeneghetti, M.C., Molin, G.M., and Tazzoli, V. (1989): X-ray diffraction study of Fe-Mg order-disorder in orthopyroxene. Some kinetic results. Physics and Chemistry of Minerals, 16, 421-427.

Schlenz, H. (1995): Orthopyroxene als potentielle Geospeedometer. PhD. dissertation, Westfa□lische Wilhelms-Universita□t Münster.

Schwandt, C.S., Cygan, R.T., and Westrich, H.R. (1998) Magnesium self-diffusion in orthoenstatite. Contributions to Mineralogy and Petrology, 130, 390-396.

Skemer, P., and Karato, S.-I. (2007) Effects of solute seggregation on the grain-growth kinetics of orthopyroxene with implications for the deformation on the upper mantle. Physics of the Earth and Planetary Interiors, 164, 186-196.

Skogby, H. (1992): Order-disorder kinetics in orthopyroxenes of ophiolite origin. Contributions to Mineralogy and Petrology, 109, 471-478.

Smith, D., and Barron, B.R. (1991) Pyroxene-garnet equilibration during cooling in the mantle. American Mineralogist, 76, 1950-1963.

Stimpfl, M., Ganguly, J., and Molin, G. (2005) Kinetics of Fe^{2+}–Mg order–disorder in orthopyroxene: experimental studies and applications to cooling rates of rocks. Contributions to Mineralogy and Petrology, 150, 319-334.

Von Seckendorff, V., and O'Neill, H.St.C. (1993) An experimental study of Fe-Mg partitioning between olivine and orthopyroxene at 1173, 1273 and 1423 K and 1.6 GPa. Contributions to Mineralogy and Petrology, 113, 196-207.

Von Seckendorff, V., O'Neill, H.St.C., Zipfel, J., and Palme, H. (1992) Evidence for a late reducing event in IAB-silicate inclusions. Meteoritics, 27, 288-289.

Vogt, K., Dohmen, R., and Chakraborty, S. (2015) Fe-Mg diffusion in spinel: New experimental data and a point defect based model. American Mineralogist, 100, 2112-2122.

Watson, E.B., and Dohmen, R. (2010) Non-traditional and emerging methods for characterizing diffusion in minerals and mineral aggregates. Reviews in Mineralogy and Geochemistry 72, 61-105

Wang, L., Moon, N., Zhang, Y., Dunham, W.R., and Essene, E.J. (2005) Fe-Mg order-disorder in orthopyroxenes. Geochimica et Cosmochimica Acta, 69, 5777-5788.

Zhukova, I., O'Neill, H.St.C., Cambell, I.H., and Kilburn, M.R. (2014) The effect of silica activity on the diffusion of Ni and Co in olivine. Contributions to Mineralogy and Petrology, 168:1029, DOI 10.1007/s00410-014-1029-z.

Ziegler, J.F., and Manoyan, J.M. (1988) The stopping of ions in compounds. Nuclear Instruments Methods, B35, 215-228.

Tables

Table 1

	OPX7 batch 1	**OPX7 batch 2**	**OPX8 batch 1**	**OPX8 batch 2**
wSiO2	58.08 ± 0.20	58.75 ± 0.25	58.48 ± 0.35	59.56 ± 0.32
wMgO	34.91 ± 0.13	34.91 ± 0.14	38.52 ± 0.18	38.34 ± 0.14
wFeO	6.37 ± 0.10	6.28 ± 0.09	0.84 ± 0.06	1.02 ± 0.01
wMnO	0.24 ± 0.03	0.24 ± 0.02	0.08 ± 0.03	0.07 ± 0.01
wCaO	0.13 ± 0.03	0.15 ± 0.01	0.22 ± 0.02	0.27 ± 0.01
wAl2O3	0.10 ± 0.01	0.12 ± 0.01	0.82 ± 0.08	1.02 ± 0.01
wTiO2	0.04 ± 0.02	0.05 ± 0.02	0.02 ± 0.01	0.02 ± 0.01
wNa2O	0.02 ± 0.01	0.04 ± 0.01	0.02 ± 0.01	0.04 ± 0.01
wCr2O3	0.02 ± 0.02	0.02 ± 0.01	0.01 ± 0.01	0.01 ± 0.01
wK2O	0.01 ± 0.01	0.01 ± 0.01	0.01 ± 0.01	0.00 ± 0.01
wNiO	-	0.02 ± 0.02	-	0.02 ± 0.02
wV2O3	-	0.01 ± 0.01	-	0.01 ± 0.01
wTotOx	99.92 ± 0.28	100.59 ± 0.36	99.02 ± 0.48	100.37 ± 0.22
Si	1.0004	1.0042	0.9917	0.9961
Mg	0.8964	0.8894	0.9738	0.9558
Fe	0.0917	0.0898	0.0120	0.0142
Mn	0.0036	0.0035	0.0012	0.0010
Ca	0.0024	0.0027	0.0040	0.0049
Al	0.0019	0.0024	0.0164	0.0200
Na	0.0008	0.0013	0.0007	0.0013
Ti	0.0006	0.0006	0.0002	0.0002
Cr	0.0002	0.0003	0.0002	0.0001
K	0.0001	0.0002	0.0001	0.0001
Ni	-	0.0002	-	0.0002
V	-	0.0002	-	0.0002
SU1	0.9977	0.9906	1.0086	0.9980
O’	3	3	3	3
En	90.1	90.2	98.2	97.9
Fs	9.2	9.1	1.2	1.5

Table 2 Experimental conditions and measured diffusion coefficients.

Run#	T (°C)	t (min)	log[fO_2(Pa)]*		sample	o#	log[D(m^{2}s^{-1})]			sample	log[D(m^{2}s^{-1})]		
OPXD_01	1000	1200	-7	-7.0	7D_02	//c	-19.01	±	0.08	8D_03	-19.29	±	0.04
OPXD_02	1000	3821	-7	-7.0	7D_04	//c	-19.09	±	0.21	8D_06	-19.29	±	0.05
OPXD_03	905	4145	-7	-7.3	7D_07	//c	-19.89	±	0.04	8D_07	-20.69	±	0.03
OPXD_04	946	4356	-7	-6.7	7D_10	//c	-19.79	±	0.06	8D_10	-19.69	±	0.08
OPXD_05	1043	1200	-7	-6.7	7D_11	//c	-18.79	±	0.12	8D_11	-19.04	±	0.06
OPXD_07	996	2540	-9	-8.4	7D_13	//c	-18.79	±	0.05	8D_13	-19.49	±	0.04
OPXD_09	996	3939	-11	-11.0	7D_15	//c	-19.54	±	0.09	8D_15	-19.69	±	0.06
OPXD_10	1094	248	-7	-6.0	7D_16	//c	-18.14	±	0.08	8D_16	-18.04	±	0.09
OPXD_12	894	4400	-11	-9.4	7D_18	//c	-20.24	±	0.05	8D_18	-20.89	±	0.04
OPXD_13	948	2701	-11	-11.2	7D_19	//c	-19.69	±	0.06	8D_19	-20.24	±	0.04
OPXD_14	950	4001	-7	-7.0	7D_20	//c	-19.49	±	0.07	8D_21			
					7D_21	//c	-19.59	±	0.07				
OPXD_15	993	775	-7	-7.0	7D_22	//c	-19.14	±	0.11	8D_23	-19.44	±	0.04
OPXD_21	904	7062	-11	-11.2	7D_28	//c	-20.64	±	0.06	8D_29			
OPXD_23	872	10324	-11	-11.4	7D_30	//c	-20.34	±	0.04	8D_31	-20.69	±	0.04
					7D_31	//c	-20.59	±	0.05				
OPXD_24	928	5054	-11	-11.1	7D_32	//c	-19.99	±	0.05	8D_32	-20.09	±	0.03
OPXD_25	1048	332	-7	-6.7	7D-2-1	//a	-19.01	±	0.05				
					7Db02	//	-18.71	±	0.05				
OPXD_26	999	1330	-7	-7.0	7D-2-2	//a	-19.61	±	0.05				
					7Db03	//	-19.31	±	0.06				
OPXD_29	993	1380	-7	-7.3	7Dr29	//c	-19.01	±	0.07				
					7Da03	//a	-19.30	±	0.07				
OPXD_30	1043	1373	-7	-7.1	7Dr26	//c	-18.45	±	0.06				
					7Da04	//a	-19.20	±	0.06				
OPXD_31	942	4330	-7	-7.8	7Dr24	//c	-19.65	±	0.12				
					7Da05	//a	-20.15	±	0.07				
OPXD_32	1104	83	-8	-7.9	7D-1N1	//c	-17.85	±	0.06				
OPXD_33	1103	86	-7	-7.0	7D-1N2	//c	-17.89	±	0.06				

* Left value is the nominal fO_2 as given by the controlled CO/CO_2 and the right value is those fO_2 as measured by the ZrO_2 sensor.
# Diffusion direction

Figure captions

Figure 1: RBS spectra for Run# =OPXD-23 (a) Samples Opx7D_30 + Opx7D_32_Ref. and (b) corresponding extracted Fe concentration depth profiles. Four different types of fits are shown in (b) using different exponents to describe the compositional dependence: n = 0, 1, 2, and 3. The respective values for D of Opx7 composition (X_{Fe} = 0.09) are given in the additional legend as inset in the figure.

Figure 2: Surface characterization of samples Opx7D_13 and Opx8D_13 from Run# =OPXD-07 using reflected light microscopy (a, b), phase shift interference light microscope (c, d), and secondary electron microscopy (e, f), respectively.

Figure 3: Measured $D_{Fe\text{-}Mg}$ for Opx7 and Opx8 at four and three different run durations, respectively, at 993 °C and 1000 °C and $fO_2 = 10^{-7}$ Pa. Note that for activation energies within 200-400 kJ/mol the change in $D_{Fe\text{-}Mg}$ induced by a T change of 7 °C is within the reported error bars.

Figure 4: Arrhenius plot of $D_{Fe\text{-}Mg}$ measured for (a) Opx7 (at the nominal $fO_2 = 10^{-7}$ Pa and $fO_2 = 10^{-11}$ Pa) and (b) Opx8. Solid lines are linear regressions of the data according to Eqn. 1 but by assuming n = 0 for Opx8 and by fixing the activation energy at the value obtained for experiments //[001] for fitting $D_{Fe\text{-}Mg}$ data measured //[100]. .

Figure 5: Comparison of $D_{Fe\text{-}Mg}$ of Opx7 (Fs_9) as predicted according to Eqn. 1 for log fO_2 [Pa] = -7 (solid lines), as well as variable fO_2 along the NNO (dotted line), and IW (dashed line) buffers. Data points for Mg tracer diffusion coefficients measured by [1] Schwandt et al. (1988) at fO_2 = IW, Fs_{11}, are plotted as symbols. Different symbols are used for data from different crystallographic directions, as described in the legend. Raw data of Schwandt et al. (1998) are shown instead of a fit to the data to illustrate that the diffusional anisotropy of D_{Mg} is not well resolved with this data set. The data set of Schwandt et al. (1988) can be well described by Eqn (1) which has only a weak dependence on fO_2. $D_{Fe\text{-}Mg}$ for Fs_9 calculated using expressions from Ganguly and Tazzoli (1994) at IW buffer [2], and from Allan et al. (2013) at NNO buffer [3] are also shown for comparison. Additionally, the inset shows calculated values of $D_{Fe\text{-}Mg}$ for Fs_9 using the expression given by Allan et al. (2013) at a constant oxygen fugacity of log fO_2 [Pa] = -11 compared to our results at log fO_2 [Pa] = -11 and log fO_2 [Pa] = -7. These results shows how the strong fO_2 dependence of diffusivity postulated by Allan et al. (2013) (Eqn. 3) leads to a low activation energy and significant deviation from measured values at many temperatures.

Figure 6: Measured ordering (and some disordering) rates (reaction constant K^+) for orthopyroxene at various fO_2 and various contents of X_{Fs} as indicated at the lines or in the legend within the figure. The ordering rates measured by isothermal experiments for ranges of X_{Fs} = 0.39 – 0.51 and X_{Fs} = 0.09 – 0.19 are from various sources: Besancon (1981), Saxena et al. (1987, 1989), and Schlenz (1995). In addition, ordering data of Anovitz et al. (1988) are shown (not the individual data points were given there but only a bulk fit, as shown here) as well as the recalculated ordering rates of Anovitz et al. (1988) as determined by Krot et al. (1997). The respective change in ordering rate is indicated by an arrow. Upwards and downwards oriented triangles are the data points for ordering and disordering rates, respectively, of orthopyroxene of Fs_{50} composition, as determined by isothermal experiments of Stimpfl et al. 2005. Note that the single data point measured for fO_2 = NNO directly coincides with the disordering rate measured

at the same temperature but for an fO_2 = IW. The ordering rate measured for Opx with Fs_{16} (long dashes) of Stimpfl et al. (2005) was measured by cooling experiments and thus required various assumptions to reconstruct the ordering rate at a given temperature. Also shown are calculated reaction constants using Equation 4 and $D_{Fe\text{-}Mg}$ from Equation 1 for Opx7 (Fs_9) at fO_2 = IW (solid line). The two additional lines (long dash-dotted and short dash-dotted) are ordering rates as predicted form the simultaneous fit of various data by Krot et al. (1997) for X_{Fs} = 0.1 and X_{Fs} = 0.5. Note the overall limited range of ordering rates at a given temperature (grey area) indicating a small effect of fO_2 as well as X_{Fs}. Notable exceptions are the data of Stimpfl et al. (2005) for X_{Fs} = 0.16 and the original uncorrected data of Anovitz et al. (1988).

Figure 7: Comparison of $D_{Fe\text{-}Mg}$ of Opx7 (solid lines, as predicted for fO_2 = IW) and Opx8 (dashed line) with other experimentally measured diffusion coefficients of various cations for orthopyroxene: [1] – D_{Mg} (tracer diffusion at fO_2 = IW, Fs_{11}; Schwandt et al. 1998); [2] – D_{Cr}, fO_2 = IW, Fs_3 (Ganguly et al. 2007); [3] – D_{Gd} in air, Fs_1, [4] – D_{Eu3+} in air, Fs_1, [5] – D_{Eu2+}, fO_2 = IW, Fs_1 (Cherniak and Liang 2007); [6] – D_{Nd}, fO_2 = WM, Fs_2 (Sano et al. 2011); [7] – D_{Ti}, various fO_2, Fs_1 (Cherniak and Liang 2012); [8] – D_{Pb}, fO_2 = QFM, Fs_1 (Cherniak 2001). Crystallographic orientation of the diffusion flux in each experimental data set is indicated beside the respective Arrhenius line.

Figure 8: Comparison of $D_{Fe\text{-}Mg}$ for //[001] in orthopyroxene with data from the literature for $D_{Fe\text{-}Mg}$ of //[001] in olivine, //[001] in clinopyroxene, spinel and garnet. For both orthopyroxene (this study) and olivine (e.g., Dohmen et al. 2007) the c-axis was identified as the fastest diffusion direction. Diffusion in cubic spinel and garnet is isotropic. Major element composition (content of the Fe-bearing endmember) and data source is indicated at each line. The data are shown for the T range and P, fO_2 conditions of the respective experiments. The exception is garnet where $D_{Fe\text{-}Mg}$ of Borinski et al. (2012) was normalized to P = 0.1 MPa from 2.5 GPa using the reported pressure dependence. Orthopyroxene – P = 0.1 MPa, , log (fO_2 [Pa]) = -11; Clinopyroxene – P = 0.1 MPa, no fO_2 dependence found (Mueller et al. 2013); Spinel – P = 2.1 GPa (Liermann and Ganguly 2002) and P = 0.1 MPa, log (fO_2 [Pa]) = -12 (Vogt et al. 2015); Olivine – P = 0.1 MPa, log (fO_2 [Pa]) = -7. Note that the fO_2 in the piston cylinder experiments of Liermann and Ganguly (2002) and Borinski et al. (2012) is defined by the graphite furnace and pressure cell design (see discussion in the respective original papers).

This is a preprint, the final version is subject to change, of the American Mineralogist (MSA)
Cite as Authors (Year) Title. American Mineralogist, in press.
(DOI will not work until issue is live.) DOI: http://dx.doi.org/10.2138/am-2016-5815

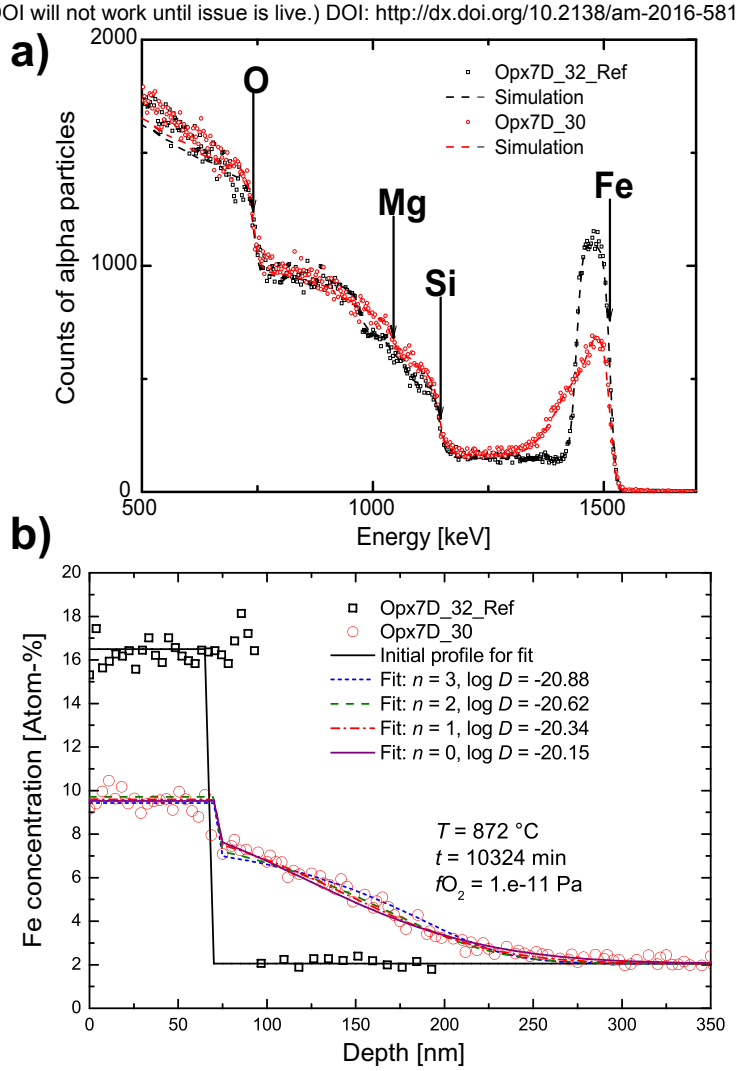

Figure 1

This is a preprint, the final version is subject to change, of the American Mineralogist (MSA)
Cite as Authors (Year) Title. American Mineralogist, in press.
(DOI will not work until issue is live.) DOI: http://dx.doi.org/10.2138/am-2016-5815

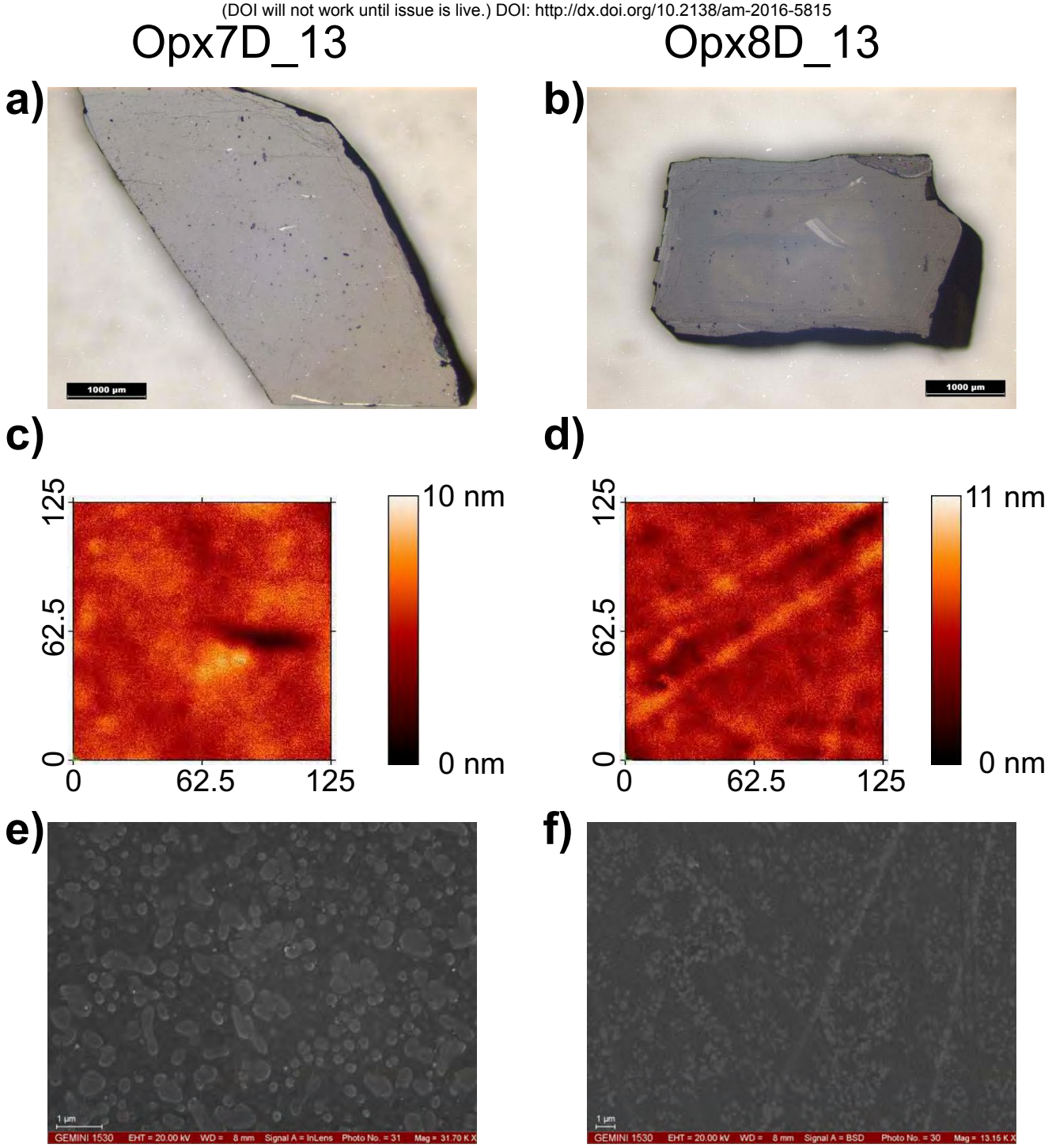

Figure 2

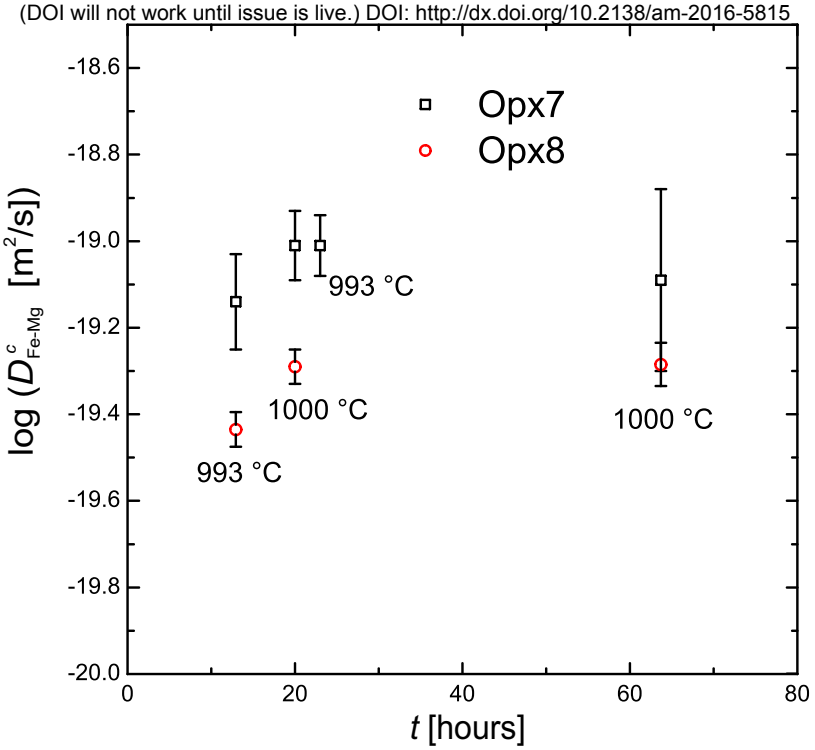
Opx7
Opx8
993 °C
1000 °C
993 °C
1000 °C
-18.6
-18.8
-19.0
-19.2
-19.4
-19.6
-19.8
-20.0
0
20
40
60
80
t [hours]
log (D^c_{Fe-Mg} [m^2/s])

Figure 3

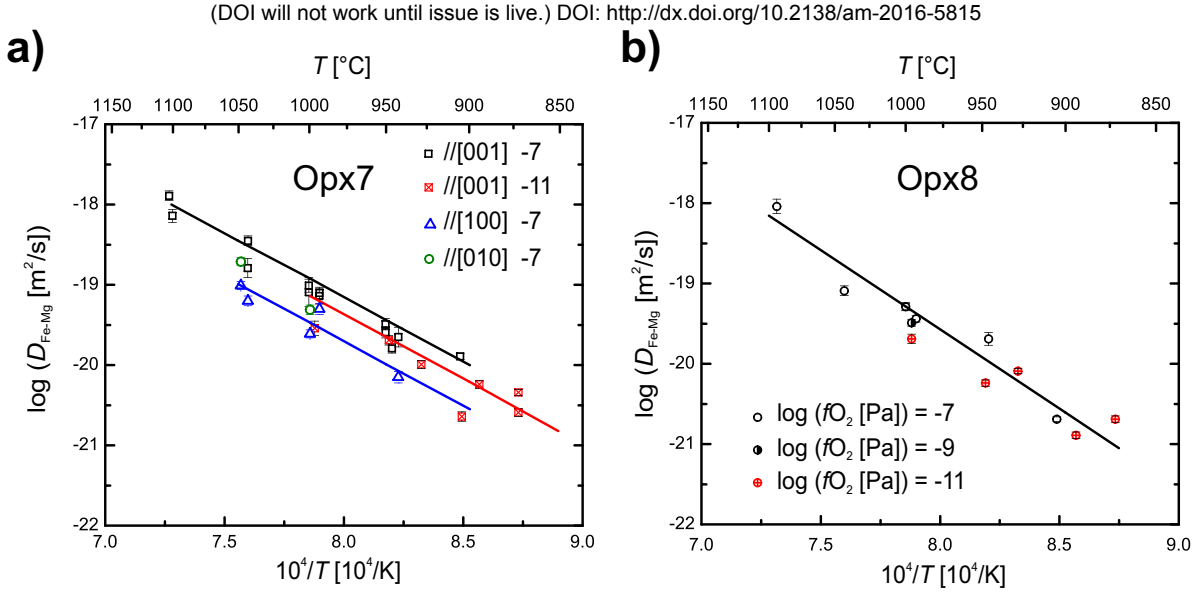
a)
T [°C]
1150 1100 1050 1000 950 900 850
Opx7
//[001] -7
//[001] -11
//[100] -7
//[010] -7
log (D_{Fe-Mg} [m^2/s])
-17 -18 -19 -20 -21 -22
7.0 7.5 8.0 8.5 9.0
$10^4/T$ [10^4/K]
b)
T [°C]
1150 1100 1050 1000 950 900 850
Opx8
log (fO_2 [Pa]) = -7
log (fO_2 [Pa]) = -9
log (fO_2 [Pa]) = -11
log (D_{Fe-Mg} [m^2/s])
-17 -18 -19 -20 -21 -22
7.0 7.5 8.0 8.5 9.0
$10^4/T$ [10^4/K]

Figure 4

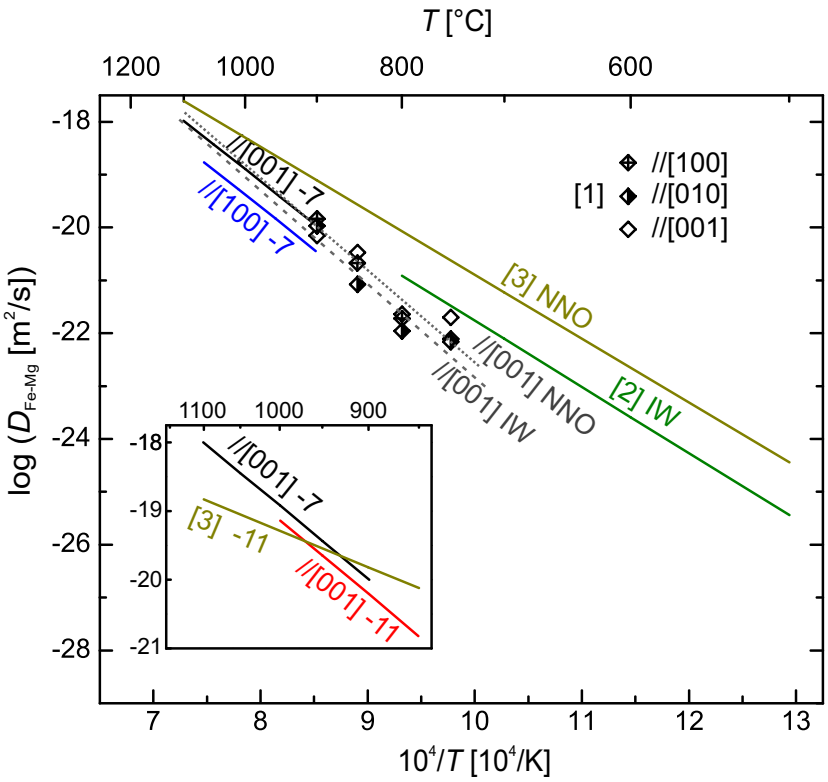
T [°C]
1200
1000
800
600
-18
-20
-22
-24
-26
-28
log (D_{Fe-Mg} [m²/s])
7
8
9
10
11
12
13
$10^4/T$ [10^4/K]
//[100]
[1] //[010]
//[001]
//[001] -7
//[100] -7
[3] NNO
[2] IW
//[001] NNO
//[001] IW
1100
1000
900
-18
-19
-20
-21
//[001] -7
[3] -11
//[001] -11

Figure 5

This is a preprint, the final version is subject to change, of the American Mineralogist (MSA)
Cite as Authors (Year) Title. American Mineralogist, in press.
(DOI will not work until issue is live.) DOI: http://dx.doi.org/10.2138/am-2016-5815

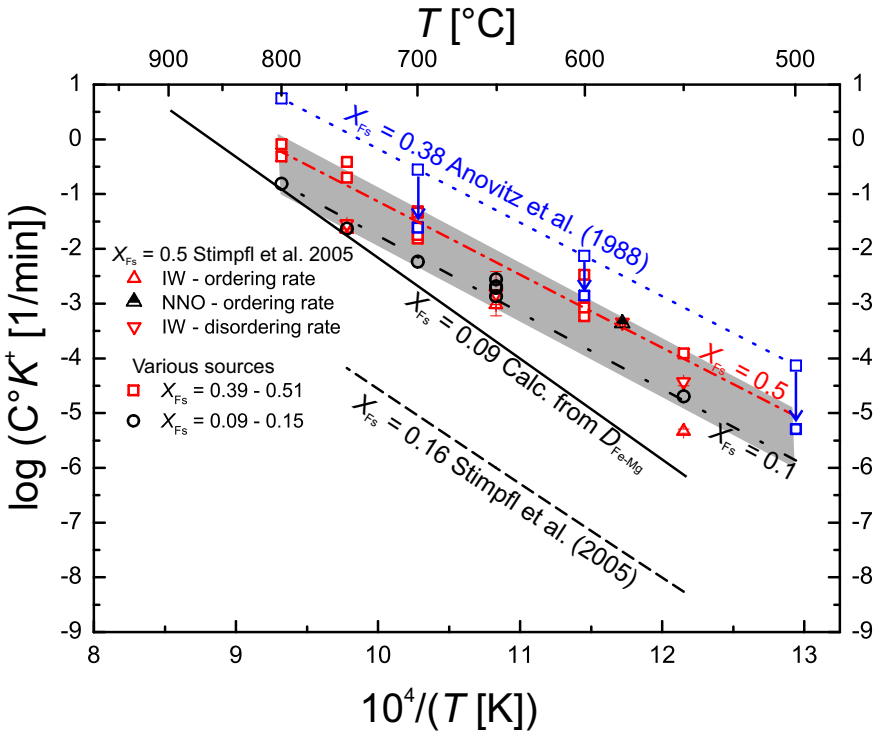

Figure 6

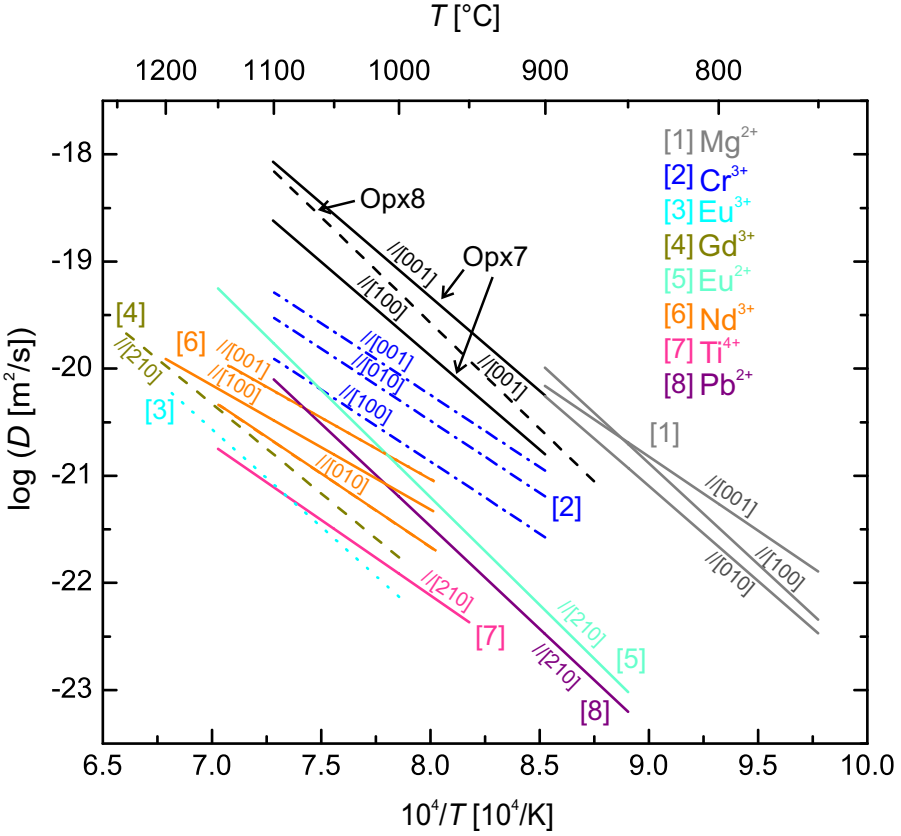
T [°C]
1200
1100
1000
900
800
-18
-19
-20
-21
-22
-23
log (D [m²/s])
6.5
7.0
7.5
8.0
8.5
9.0
9.5
10.0
10⁴/T [10⁴/K]
[1] Mg2+
[2] Cr3+
[3] Eu3+
[4] Gd3+
[5] Eu2+
[6] Nd3+
[7] Ti4+
[8] Pb2+
Opx8
Opx7
//[001]
//[100]
//[010]
//[210]
[1]
[2]
[3]
[4]
[5]
[6]
[7]
[8]

Figure 7

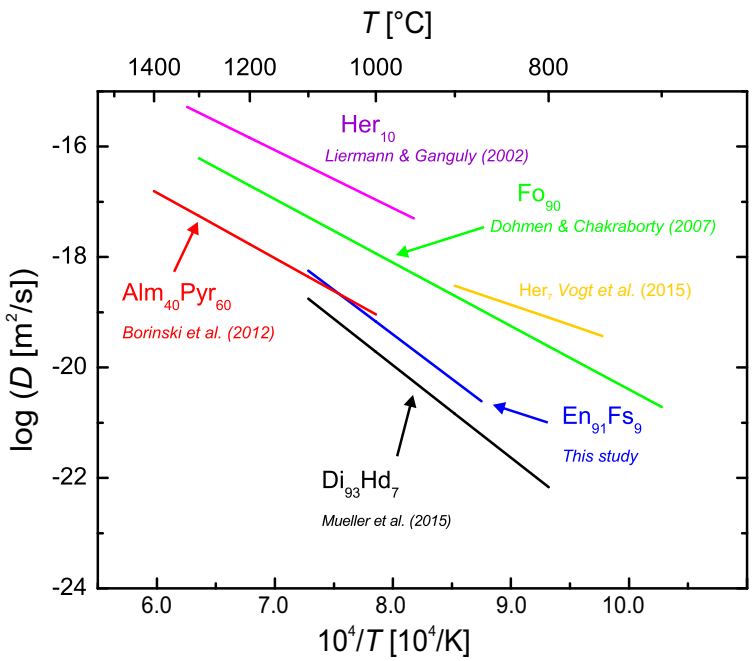
T [°C]
1400
1200
1000
800
Her10
Liermann & Ganguly (2002)
Fo90
Dohmen & Chakraborty (2007)
Her, Vogt et al. (2015)
Alm40Pyr60
Borinski et al. (2012)
En91Fs9
This study
Di93Hd7
Mueller et al. (2015)
log (D [m2/s])
-16
-18
-20
-22
-24
6.0
7.0
8.0
9.0
10.0
104/T [104/K]

Figure 8